

# Numerical study on reflection of an oblique detonation wave on an outward turning wall

Cite as: Phys. Fluids **32**, 046101 (2020); <https://doi.org/10.1063/5.0001845>

Submitted: 20 January 2020 . Accepted: 16 March 2020 . Published Online: 01 April 2020

Kuanliang Wang (王宽亮) , Zijian Zhang (张子健) , Pengfei Yang (杨鹏飞) , and Honghui Teng (滕宏辉) 



View Online



Export Citation



CrossMark

## ARTICLES YOU MAY BE INTERESTED IN

[Three-dimensional simulations of detonation propagation in circular tubes: Effects of jet initiation and wall reflection](#)

Physics of Fluids **32**, 046104 (2020); <https://doi.org/10.1063/1.5143105>

[Development of a stagnation streamline model for thermochemical nonequilibrium flow](#)

Physics of Fluids **32**, 046102 (2020); <https://doi.org/10.1063/5.0003247>


[Effects of the fresh mixture temperature on thermoacoustic instabilities in a lean premixed swirl-stabilized combustor](#)

Physics of Fluids **32**, 047101 (2020); <https://doi.org/10.1063/1.5133859>



**NEW!**

Sign up for topic alerts  
New articles delivered to your inbox



# Numerical study on reflection of an oblique detonation wave on an outward turning wall

Cite as: *Phys. Fluids* **32**, 046101 (2020); doi: [10.1063/5.0001845](https://doi.org/10.1063/5.0001845)

Submitted: 20 January 2020 • Accepted: 16 March 2020 •

Published Online: 1 April 2020





View Online



Export Citation



CrossMark

Kuanliang Wang (王宽亮),<sup>1</sup>  Zijian Zhang (张子健),<sup>2,3</sup>  Pengfei Yang (杨鹏飞),<sup>2,3</sup>   
and Honghui Teng (滕宏辉)<sup>1,a)</sup> 

## AFFILIATIONS

<sup>1</sup>School of Aerospace Engineering, Beijing Institute of Technology, Beijing 100081, China

<sup>2</sup>State Key Laboratory of High Temperature Gas Dynamics, Institute of Mechanics, Chinese Academy of Sciences, Beijing 100190, China

<sup>3</sup>School of Engineering Sciences, University of Chinese Academy of Sciences, Beijing 100049, China

<sup>a)</sup> Author to whom correspondence should be addressed: [hhteng@bit.edu.cn](mailto:hhteng@bit.edu.cn)

## ABSTRACT

Oblique detonation waves (ODWs) have been studied widely as the basis of detonation-based hypersonic engines, but there are few studies on ODWs in a confined space. This study simulates ODW reflection on a solid wall before an outward turning corner for a simplified combustor–nozzle flow based on a two-step kinetic model. Numerical results reveal three types of ODW structures: stable, critical, and unstable. When the reflection occurs at the turning point, the stable ODW structure remains almost the same as before reflection. When the wave reflects at the wall before the turning point, either the critical structure or the unstable structure arises, which has never been investigated before. Both structures have the same initial two-section detonation surface: but the critical one becomes stationary at a certain position, while the unstable one keeps traveling upstream. By adjusting the location of the expansion wave and degree of the turning angle, the difference of the two structures is attributed to the thermal choking appearing only in the unstable structure. The thermal choking is achieved by the merging of subsonic zones, whose dependence on the various parameters is discussed.

Published under license by AIP Publishing. <https://doi.org/10.1063/5.0001845>

## I. INTRODUCTION

A current frontier of aeronautic engineering is developing air-breathing propulsion systems<sup>1–5</sup> for hypersonic aircrafts. Detonation-based engines<sup>6–9</sup> are a new propulsion concept featuring high thermal efficiency based on pressure-gain combustion. One type of detonation-based engine that is attracting increasing attention is the oblique detonation engine (ODE), which is suitable for air-breathing hypersonic propulsion. However, it is not easy to harness the oblique detonation wave (ODW) in the high-speed inflow, and the structure and stability of the ODW needs to be clarified first by addressing the complicated interaction of shock, heat release, and geometry.

Early research on ODWs<sup>10</sup> used a spherical projectile launched into a combustible mixture, which can initiate an ODW with a relatively low Mach number because of the appearance of normal shock in front of the blunt surface. Later studies reproduced the phenomenon numerically<sup>11,12</sup> and experimentally,<sup>13,14</sup> revealing

the structural features and mechanism of combustion instability.<sup>15</sup> Meanwhile, the straight oblique shock wave (OSW), induced by the presence of a wedge or ramp in the supersonic flow, has been predominantly used in engines. The OSW decreases the drag force from the normal shock or detonation. The ODW has traditionally been treated as an OSW with instant heat release.<sup>16,17</sup> However, this treatment is an oversimplification as found by numerical<sup>18</sup> and experimental<sup>19</sup> studies of the initiation region. The transition from the OSW to ODW could be viewed as ODW initiation. Two types of this initiation, smooth and abrupt, have been observed and analyzed in depth.<sup>20–22</sup> The instability of the ODW surface has also been studied on the basis of the transition from the straight OSW to the ODW.<sup>23–26</sup>

The aforementioned studies assumed a 2D semi-infinite wedge or ramp, but a more realistic geometric confinement should be included to promote application. Because the projectile is usually axisymmetric, studies have been done on ODWs triggered by conical shock, revealing more sophisticated initiation and

cellular structures.<sup>27,28</sup> By eliminating the assumption of a semi-infinite wedge or ramp, Papalexandris<sup>29</sup> found that the expansion wave derived from the wedge rear may quench the ODW. Further studies<sup>30,31</sup> on finite wedges found that rear expansion waves could affect detonation instability and structure. ODWs triggered by a double ramp were also analyzed to explore the possibility of wave configuration inside the detonation combustor.<sup>32</sup> However, the confinement of the combustor geometry, such as the upper wall of the flow tunnel, has not been considered so far. This brings difficulties and uncertainties to the combustor design, which needs a stabilized ODW in a limited space.

This study simulates the ODW in a flow tunnel, focusing on ODW reflection on the upper wall. The upper wall has an outward turn, a simplified model of the combustor–nozzle flow in ODEs. Previous studies<sup>33,34</sup> have considered the ideal situation in which the ODW reflects at the turning point, so the structure is simple and stable. Beyond that ideal case, this study investigates a series of realistic cases in which the reflection occurs before the turning point. This study finds that reflection before the turning point, which is unavoidable in reality, changes the whole wave structure owing to the complicated interaction among the shock wave, heat release, and expansion wave. Three types of wave structures are observed, containing two structures not investigated before, which are named the critical or the unstable structure. Their transition mechanisms are analyzed in terms of the inflow Mach number, outward turning angle, and location of the expansion wave. Some comments on these structural findings on the application of ODW-based engines have been given in Sec. IV.

II. METHOD

Figure 1 shows the physical model and main parameters of the ODE and the computational domain. The simplified ODE geometry

studied is illustrated in Fig. 1(a) in which the ODW is first reflected by the combustor upper wall and then affected by the expanding nozzle. The corresponding computational parameters with an outward turning wall in Fig. 1(b) were used to simulate the combustor–nozzle flow. To ensure the ODW reflected before the expansion wave, the original ODW position was first captured with no upper wall there, and then, the upper wall was applied with different turning angles and turning point positions along the  $x$  axis to investigate the flow state. In this study,  $L_t$  denotes the length of the upper wall from the original, undisturbed ODW position to the turning point;  $L_s$  is the distance between the final surface and the original location;  $\theta_1$  and  $\theta_2$  are the angles of the wedge and the outward turning wall, respectively; and  $H$  is the entrance inflow height. There is also an expansion wave from the wedge or ramp, but it is far enough downstream to have a slight effect.

The simulation is based on the Euler equations with a two-step kinetic model to simplify chain-branching kinetics.<sup>35</sup> The induction reaction index  $\xi$  and heat release reaction index  $\lambda$  are the two key reaction variables for the transport equations

$$\frac{\partial(\rho\xi)}{\partial t} + \frac{\partial(\rho u\xi)}{\partial x} + \frac{\partial(\rho v\xi)}{\partial y} = H(1 - \xi)\rho k_I \exp\left[E_I\left(\frac{1}{T_s} - \frac{1}{T}\right)\right], \tag{2.1}$$

$$\frac{\partial(\rho\lambda)}{\partial t} + \frac{\partial(\rho u\lambda)}{\partial x} + \frac{\partial(\rho v\lambda)}{\partial y} = [1 - H(1 - \xi)]\rho(1 - \lambda)k_R \exp\left[\left(-\frac{E_R}{T}\right)\right] \tag{2.2}$$

with the Heaviside step function

$$H(1 - \xi) = \begin{cases} 1, & \xi \leq 1 \\ 0, & \xi > 1. \end{cases} \tag{2.3}$$

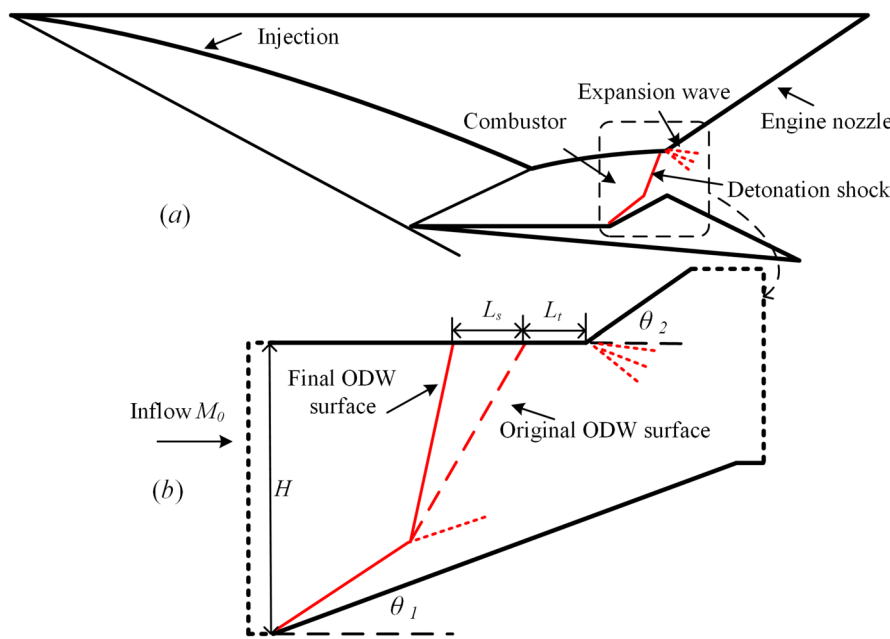


FIG. 1. Schematic of the oblique detonation engine (a) and computational domain (b).

The equation of state should be changed to include the effects of heat release, depending on the second step index  $\lambda$  rather than  $\xi$ ,

$$e = \frac{p}{\rho(\gamma - 1)} + \frac{1}{2}(u^2 + v^2) - \lambda Q. \quad (2.4)$$

It should be noted that neglecting the diffusion effects may introduce some errors, but we still keep using Euler equations in this study. Almost all the previous numerical studies of ODWs, e.g., Refs. 18 and 21–31, assumed an inviscid flow, so the Navier–Stokes equations could be simplified to be Euler equations. This is because  $Re$ , the Reynolds number, is usually very high in the ODW or other detonation study. In this study, as the preliminary study of ODWs in the confined space, the viscous effects are not considered to be compared with previous results. The main error is probably induced by the boundary layer, which has been studied recently.<sup>36</sup> However, we estimate that those simulations are still grid-dependence due to the resolution insufficiency. For our cases shown later,  $Re$  is on the scale of  $10^7$ , so this simplification will not bring too much error. According to the boundary layer theory,<sup>37,38</sup> the thickness near the turning point takes below 1.2% of the inflow height, but simulating it accurately will take much more computational resources. Hence, this study is performed based on Euler equations, which are solved using advection upstream splitting (AUSMPW+)<sup>39</sup> combined with a third-order Runge–Kutta algorithm. The flow parameters are normalized as follows:

$$p = \frac{\tilde{p}}{p_0}, \rho = \frac{\tilde{\rho}}{\rho_0}, T = \frac{\tilde{T}}{T_0}, u = \frac{\tilde{u}}{\sqrt{RT_0}}, v = \frac{\tilde{v}}{\sqrt{RT_0}}, \quad (2.5)$$

where  $p$ ,  $\rho$ ,  $T$ ,  $u$ , and  $v$  are the pressure, density, temperature, x-velocity, and y-velocity, respectively. The main chemical parameters are  $Q = 25$ ,  $\gamma = 1.2$ ,  $E_I = 4.0T_s$ , and  $E_R = 1.0T_s$ , where  $T_s$  is the post-shock temperature and  $Q$  is the nondimensionalized specific total energy.

In the simulations, the inflow Mach number  $M_0$  is a critical parameter for the ODW state. The three values  $M_0 = 6.5$ , 7.0, and 7.5 were used for this work. The left entrance height was set to  $H = 140$  at the location  $x = -5$ . The starting point of the wedge tip was  $x = 0$ , and the wedge angle ( $\theta_1$ ) was fixed to  $25^\circ$ . The length  $L_t$  and angle  $\theta_2$  of the outward turning wall were the controlling

parameters to vary the effect of the expansion wave. The flow field was initialized to the freestream values, whose velocities were calculated via the inflow number  $M_0$ . Slip-reflecting boundary conditions were used for the wedge, the upper wall, and the outward turning wall. The left boundary was fixed to supersonic inflow conditions. Behind the outward turning wall and at the right exit boundary, we used an outflow condition deduced from the interior. The grid and related resolution study are given in the Appendix.

### III. RESULTS AND DISCUSSION

#### A. Basic structure and ideal cases

First, the cases  $M_0 = 6.5$ , 7.0, and 7.5 were simulated as basic structures without including the effects of upper-wall confinement. Figure 2 displays the flow fields for  $M_0 = 6.5$  and 7.5 in terms of temperature and pressure. An ODW with an abrupt transition occurs for  $M_0 = 6.5$ , while an ODW with a smooth transition occurs for  $M_0 = 7.5$ . Moreover, increasing  $M_0$  causes the transition region to move upward and the angle of the ODW surface to decrease. A slip line emanates from the initiation region and extends downstream, almost parallel with the wedge surface. These wave configurations illustrate two typical ODW flow fields, similar to our previous results based on the same codes.<sup>40</sup>

The results without the upper wall were used as the basis for testing the ideal cases in which the ODW reflects exactly at the turning point. Figure 3 shows the structures with and without the upper wall for  $M_0 = 7.0$ . We first measured the position of the ODW surface in Fig. 3(a) along the line  $y = 140$  to be  $x = 155$ . Then, an upper wall was introduced along the line  $y = 140$  that turned outward at  $(150, 140)$  with a  $55^\circ$  angle deflected from the inflow direction, i.e.,  $\theta_2 = 55^\circ$ . The ODW before the turning point in Fig. 3(b) is not disturbed, but the region behind the turning point has a relatively low temperature owing to the expansion wave originating from the turning point. In contrast to the ODW in the unconfined space [Fig. 3(a)], there is no strong shock or detonation wave in the expansion region. Several other cases using different  $M_0$  and  $H$  values were simulated, indicating that these phenomena are universal for the ideal cases.

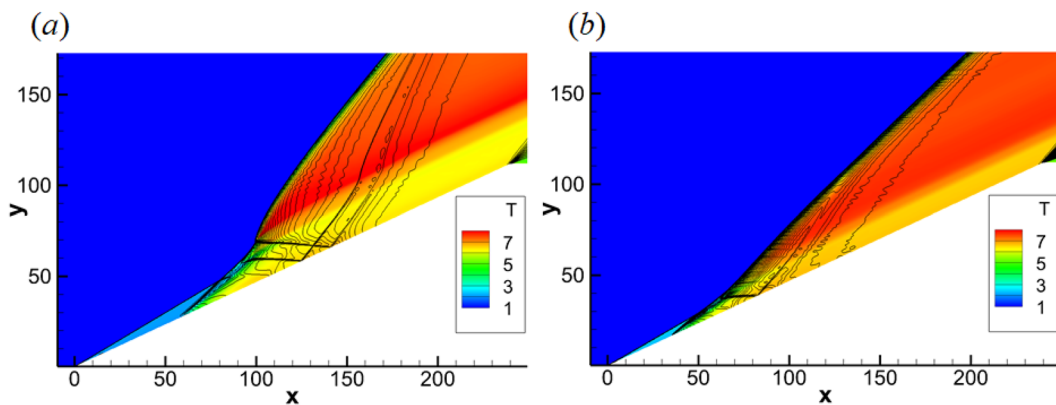


FIG. 2. Temperature fields and pressure contours (black curves) for  $M_0 = 6.5$  (a) and 7.5 (b).

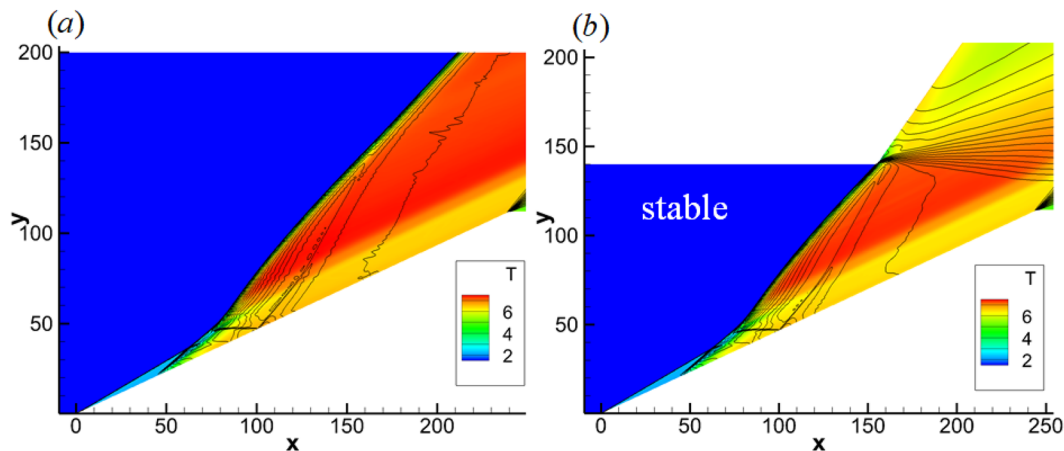


FIG. 3. Temperature fields and pressure contours (black curves) for  $M_0 = 7.0$  without the upper wall (a) and with an outward turning wall with  $\theta_2 = 55^\circ$  (b).

Owing to the lack of experimental results with which to compare directly, we performed the resolution study presented in the Appendix. The case in Fig. 3(b) was the first in the resolution study, and another case with ODW reflection was also tested. Furthermore, four sets of grids were used to examine the grid effects on the instability of the Mach stem, which will be discussed later.

### B. Structure and dynamics of nonideal cases

In ideal cases, reflection occurs exactly at the turning point. To study realistic cases in which the ODW reflects elsewhere, it is necessary to introduce the parameter  $L_t$ , defined as the distance between the undisturbed ODW (without the upper wall) and the turning point along the  $x$  direction. The ideal case, such as that of Fig. 3(b), actually corresponds to  $L_t = 0$ . If  $L_t$  is negative, the turning point is located upstream of the undisturbed ODW, so the reflection occurs in the post-expansion region. This may result in some complicated structure that has not been studied to our knowledge.

However, this study focuses on cases with positive  $L_t$  in which the ODW surface reflects on the upper wall before the turning point. This is because reflection behind the turning point occurs in a supersonic flow accelerated further by the expansion wave, so it does not affect the stationary ODW. In contrast, pre-turning reflection not only results in variation of the structure but may also change the stationary state of the structure.

The case with  $M_0 = 6.5$  and  $L_t = 5$  is shown in Fig. 4. Given a uniform inflow as the initial condition, the ODW is initiated and the angle of the ODW surface increases gradually, reaching the turning point at about  $t = 41$ . Thereafter, the surface increases further because it has not reached the equilibrium position, generating the structure in Fig. 4(a) at about  $t = 90$ . We observe that the detonation surface has two sections: one Mach stem near the upper wall and the original ODW surface. Moreover, there are many fine structures on the Mach stem, indicating that the stem is unstable. Nevertheless, the ODW of Fig. 4(a) is still transient and so propagates upstream despite the very slow speed, evolving into the structure

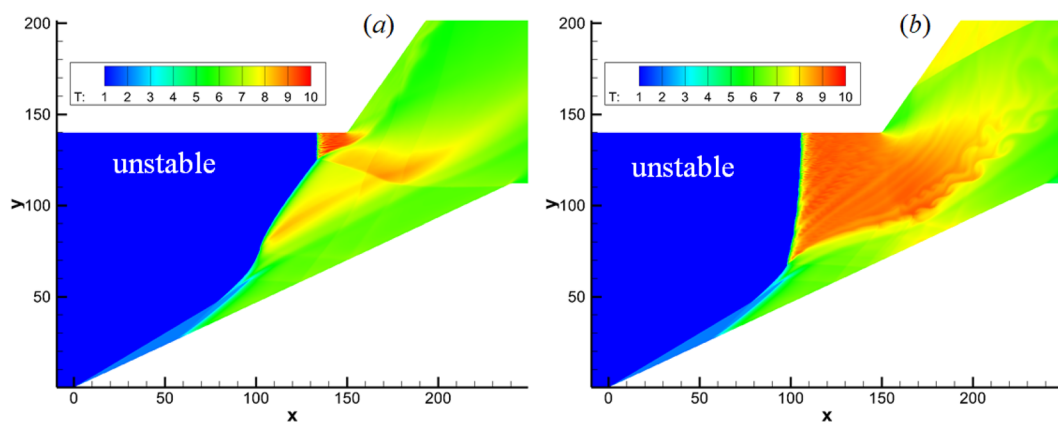


FIG. 4. Temperature for  $M_0 = 6.5$  and  $L_t = 5$  at  $t = 90$  (a) and 280 (b).

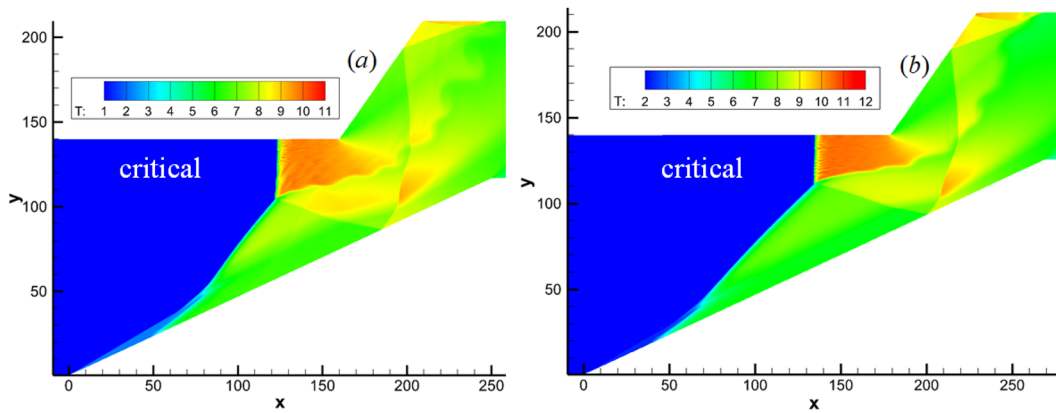


FIG. 5. Temperature for (a)  $M_0 = 7.0$  and  $L_t = 5$ ; (b)  $M_0 = 7.5$  and  $L_t = 15$ .

of Fig. 4(b). The detonation Mach stem is close to normal detonation and propagates continuously toward and beyond the inflow boundary. Decreasing  $L_t$  from 4 to 1 with  $\Delta L_t = 1$  does not change the stationary state, and the structures are similar. Therefore, it is impossible to generate a stationary ODW with positive  $L_t$ .

In contrast to the cases with  $M_0 = 6.5$ , the stationary ODW appears for certain  $L_t$  values for  $M_0 = 7.0$  and  $7.5$ . Given  $L_t = 5$  and  $M_0 = 7.0$ , a stationary ODW appears, as shown in Fig. 5(a). There is also a stationary ODW for  $L_t = 5$  and  $M_0 = 7.5$ , and Fig. 5(b) reveals a stationary ODW even after  $L_t$  increases to 15. However, numerical results indicate that these stationary structures have a similar wave configuration to that of the transient one, such as the ODW in Fig. 4(a). The ODW surface reflects on the upper wall in all cases of Figs. 5 and 4(a), generating a Mach stem with high post-shock temperature followed by an expansion wave derived from the outward turning wall. The stationary and transient structures cannot be distinguished from the wave configuration. Considering the similarity of the stationary and transient structures, we call the stationary ODW structure as the critical structure of ODW reflection.

To facilitate the analysis, the structure in each ideal case is named the stable structure, and each transient structure is named the unstable structure.

Although the critical structures appear in Fig. 5, the unstable structure appears when  $L_t$  is increased further. Figure 6 shows the structure and dynamics of two unstable ODWs with  $M_0 = 7.0$ ,  $L_t = 10$  and  $M_0 = 7.5$ ,  $L_t = 25$ . Initially, an ODW structure with Mach reflection forms quickly, as denoted by the elapsed time, and then, the surface propagates slowly upstream. The white curves show the positions of the ODW surface at different instants, indicating that the speed is not constant but variable. In both cases, the propagation velocity is slow after the two-section surface forms, but an acceleration can be observed in the later stage, denoted by the last two white curves in Fig. 6. It is impossible to explain the variation in surface velocity so far owing to the lack of comprehensive study on the wave structure. Explaining this variation needs an understanding of the underlying mechanism of the critical and unstable structures.

The length  $L_s$  is defined in Sec. II and denotes the distance from the position of ODW reflection to the turning point. Thus,  $L_s$  is a

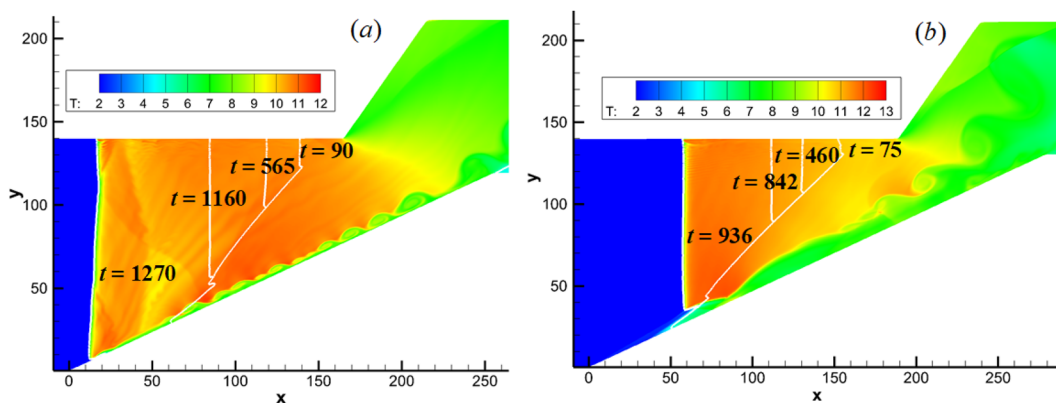


FIG. 6. Temperature for (a)  $M_0 = 7.0$  and  $L_t = 10$ ; (b)  $M_0 = 7.5$  and  $L_t = 25$ . The white curves represent the detonation surfaces at different instants.

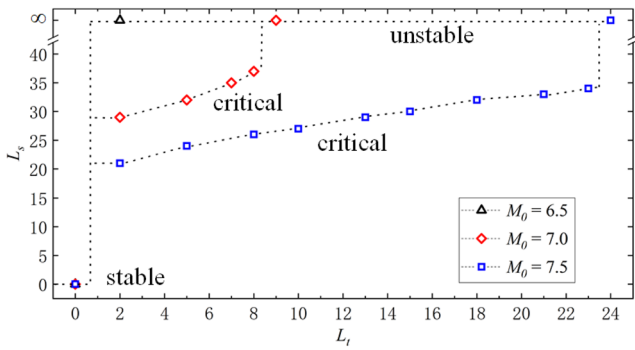


FIG. 7.  $L_s$  for ODW reflection with varying  $L_t$ .

parameter of structural instability that approaches infinity in unstable cases. To quantify and analyze the above results, we plot  $L_s$  as a function of  $L_t$  in Fig. 7. When  $L_t = 0$ , all three structures are stable, regardless of  $M_0$ . Increasing  $L_t$  may induce unstable structures when  $M_0 = 6.5$  but critical structures for  $M_0 = 7.0$  and  $7.5$ . When  $L_t$  is increased to 2,  $L_s$  jumps to about 28 for  $M_0 = 7.0$  and about 21 for  $M_0 = 7.5$ . A small variation of  $L_t$  results in a large variation of  $L_s$ , indicating a nonlinear relation derived from the structural shift. Increasing  $L_t$  above 2 introduces a slow increase in  $L_s$ , and the critical structure is observed in a range of  $L_s$ . The lower boundary of the critical structure is 0, while the upper boundary depends on  $M_0$ . The critical-to-unstable shift occurs between 8 and 9 for  $M_0 = 7.0$  and between 23 and 24 for  $M_0 = 7.5$ . These results suggest that the critical structure is related to high  $M_0$  and small  $L_s$ , but a more detailed analysis on flow fields is necessary.

C. Discussion on structural characteristics

To explore the mechanism of the critical structure, additional simulations were performed by varying the outward turning angle  $\theta_2$  and keeping  $L_t = 0$ . Numerical results indicate that the stable structures appear when  $\theta_2 = 45.0^\circ$ , regardless of  $M_0$ . When  $\theta_2$  decreases further to  $35.0^\circ$ , different types of structures appear, as shown in Fig. 8. When  $M_0 = 6.5$ , the unstable structure arises, and

Fig. 8(a) illustrates the temperature field at certain time ( $t = 330$ ). It is observed that the Mach stem is curved rather than straight and will propagate upstream subsequently. On the contrary, the Mach stem is straight and stationary when  $M_0 = 6.5$ , demonstrating a critical structure in Fig. 8(b). The sonic curves, corresponding local Mach number 1.0, are plotted in Fig. 8. For the critical structure of Fig. 8(b), there is only one subsonic zone behind the Mach stem, but there are several irregular subsonic zones in the unstable structures. Using small decrements of  $\theta_2$ ,  $\Delta\theta_2 = 0.5^\circ$ , we found the smallest angle corresponding to the stable structure to be  $41.0^\circ$ ,  $38.5^\circ$ , and  $35.5^\circ$  for  $M_0 = 6.5$ ,  $7.0$ , and  $7.5$ , respectively. Similarly to the structural shift caused by  $L_t$  variation, the structure becomes unstable for  $M_0 = 6.5$  while becoming critical for  $M_0 = 7.0$  and  $7.5$ . These results indicate that the three structures are universal and depend on both  $L_t$  and  $\theta_2$  besides  $M_0$ .

On the three structures, except for the stable structure simulated previously, there are few studies on the critical and the unstable structures in the literature. These two structures have similar wave configurations, featuring a Mach reflection of the ODW surface on the upper wall. On the basis of their different propagation features, the structure that becomes stationary at a certain position has been named the critical one and the structure that keeps traveling upstream has been named the unstable one. However, both structures have the same initial wave configuration, so it is necessary to determine the underlying differences between them.

Considering that the unstable structures have different flow fields, we first plot two critical structures of ODW reflection with sonic curves in Fig. 9. These two cases are designated critical structures but are close to the upper boundary of the critical structure. By increasing  $L_t$  further, the unstable structure appears when  $L_t = 9$  for  $M_0 = 7.0$  and  $L_t = 24$  for  $M_0 = 7.5$ . These flow fields reveal that subsonic zones exist behind the Mach stem, which ends around the outward turning point. One slip line and one oblique shock originate from the contact between the Mach stem and the undisturbed ODW surface. The slip line becomes the lower boundary of the subsonic zone, and the oblique shock, which is the secondary OSW, extends downstream and reflects on the wedge. There are two subsonic zones behind the reflection shock of the secondary OSW in both cases. These are located close to the subsonic zone behind the Mach stem. Furthermore, the subsonic zone may be generated near

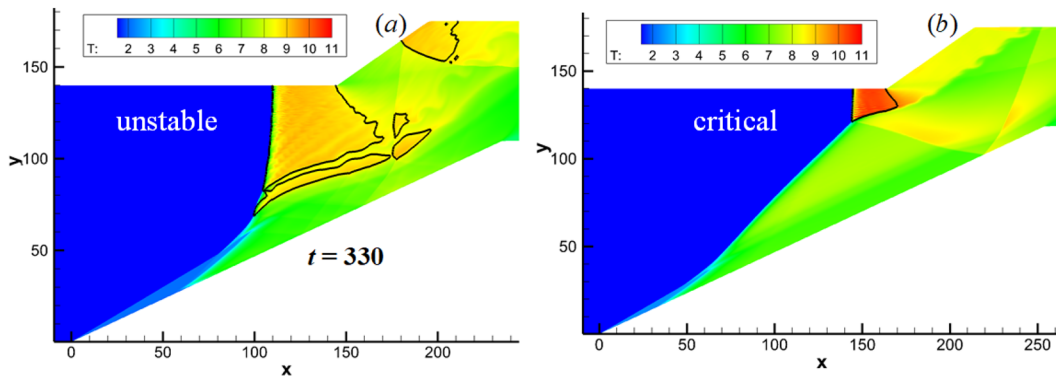
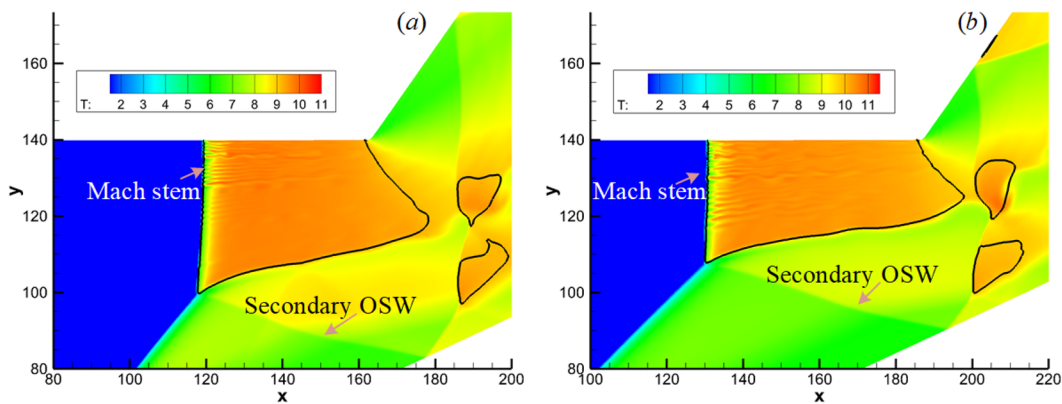


FIG. 8. Temperature with sonic curves (by black contours, corresponding local Mach number 1.0) for  $\theta_2 = 35.0^\circ$  and  $L_t = 0$ : (a)  $M_0 = 6.5$ ; (b)  $M_0 = 7.5$ .



**FIG. 9.** Temperature of the critical structure of ODW reflection with sonic curves (by black contours, corresponding local Mach number 1.0): (a)  $M_0 = 7.0$ ,  $L_t = 8$ ; (b)  $M_0 = 7.5$ ,  $L_t = 23$ .

the upper wall after the turning point, as shown in Fig. 9(b), but the zone is very small in this case. For the critical structure with low  $L_t$ , such as that in Fig. 8(b), there is only one subsonic zone behind the Mach stem. Undoubtedly, there are no subsonic zones behind the stable structures. Therefore, the formation of several subsonic zones

influences the shift from the critical structure to the unstable one significantly.

To be compared with the critical structure, the flow fields at different instants of one unstable structure are plotted in Fig. 10. This case corresponds to the one in Fig. 9(a), only increasing  $L_t$  from 8

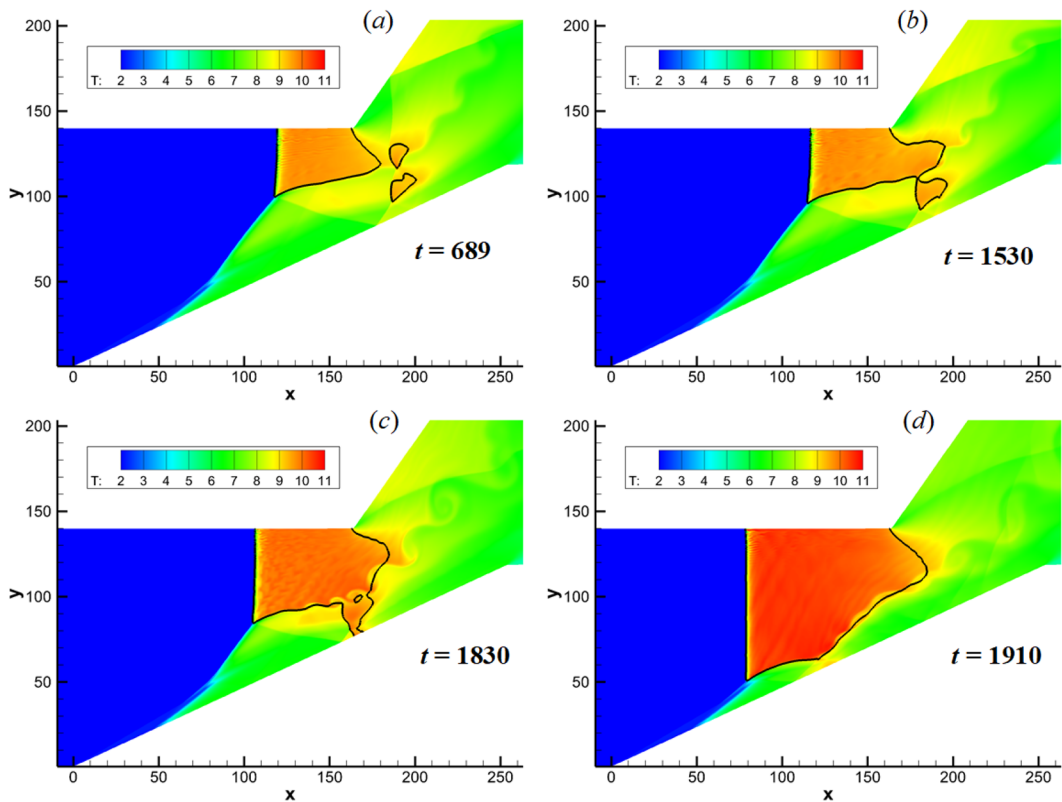


**FIG. 10.** Temperature of the unstable structure of ODW reflection with sonic curves (by black contours, corresponding local Mach number 1.0),  $M_0 = 7.0$  and  $L_t = 9$ : (a)  $t = 689$ ; (b)  $t = 1530$ ; (c)  $t = 1830$ ; (d)  $t = 1910$ .



to 9. Initially, the wave configurations are similar in Figs. 9(a) and 10(a), but we observe that the Mach stem and secondary OSW still propagate upstream slowly thereafter. After a slow evolution process, the two small subsonic zones merge with the main subsonic zone behind the Mach stem, as shown in Fig. 10(b). This merging introduces the new disturbance to the subsonic zone, destabilizing the wave system essentially. As shown in Figs. 10(c) and 10(d), the connected subsonic zone blocks the whole flow tunnel, resulting in a continuous propagation of the wave system. Comparing this evolution and the critical structure, it can be concluded that the merging of subsonic zones determines the ODW stationary, leading to either the critical structure or the unstable structure.

The schematic of the critical or unstable structure in Fig. 11 illustrates the instability mechanism. The Mach reflection induces the main subsonic zone, while the secondary OSW, with its reflection on the wall, plays the key role in the formation of other subsonic zones. The existence of more than one subsonic zone is necessary to achieve the critical-unstable shift, at least in these cases. Increasing  $L_t$  induces the unstable structure because the merging of these subsonic zones happens, caused by the post-stem subsonic zone moving downstream and the secondary OSW reflecting upstream. On the contrary, decreasing  $L_t$  eliminates the subsonic zones derived from the reflection of the secondary OSW. For example, there is only one subsonic zone in the cases  $L_t = 5$ ,  $M_0 = 7.0$  and  $L_t = 15$ ,  $M_0 = 7.5$ . From the viewpoint of subsonic zone merging, it is easy to understand the effects of  $M_0$  and  $\theta_2$ . High  $M_0$  suppresses the formation of the subsonic zone behind the reflection of the secondary OSW, so there is a wide range of  $L_t$  for critical structures. On the other side, in the cases of low  $\theta_2$ , the expansion is weak with a relatively low Mach number along the post-turning upper wall. Then, the subsonic zone easily forms and merges with the post-stem subsonic zone, inducing the unstable structure.

The merging of subsonic zones dominates the stationary state of an ODW with Mach reflection, but it is difficult to predict the criterion for the structural shift. This is because the flow is very complicated and there are still unresolved problems. The key concern for the subsonic zone is the Mach stem of the detonation surface. Studies on Mach reflection of OSWs have yielded theoretical expressions for the growth rate and steady-state height of the Mach stem.<sup>41,42</sup>

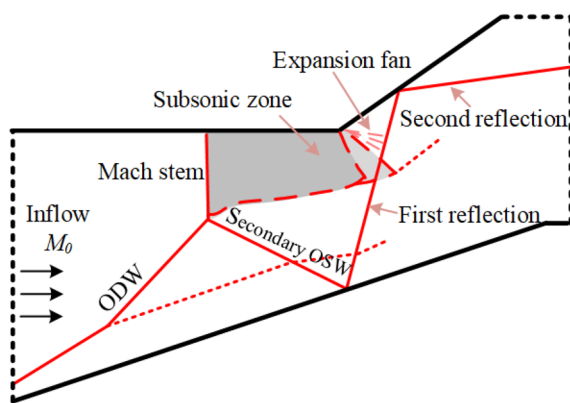


FIG. 11. Schematic of the critical or unstable structure.

However, including heat release in the detonation brings great difficulties, involving the interaction among two slip lines, three OSWs, one expansion wave, and two solid walls. Furthermore, the Mach stem is intrinsically unstable, so its features and mechanisms need further study.

#### IV. CONCLUSION

This study has simulated ODW reflection on an upper wall followed by an outward turning corner. Numerical results reveal a critical and an unstable structure beside the stable structure of the ideal case in which reflection occurs at the turning point. Both structures have the same two-section detonation surface, composed of one Mach stem near the upper wall and the undisturbed ODW surface. However, the unstable structure does not stop and results in an upstream-traveling normal detonation, while the critical one generates a stationary structure. The type of ODW structure is sensitive to  $M_0$ ,  $L_t$ , and  $\theta_2$  and becomes unstable when  $M_0$  and  $L_t$  increase but  $\theta_2$  decreases. The shift from critical to unstable structures results from thermal choking of the unstable structures, although the wave configurations of both structures are initially similar. By adjusting the location of the expansion wave and degree of the turning angle, we found that the thermal choking happens in the unstable structures. Analysis of the structural characteristics shows that the merging of subsonic zones dominates the stationary state of an ODW with Mach reflection.

The critical and unstable structures bring new challenges to the application of ODW-based engines. From the viewpoint of practical applications, a stationary ODW is necessary to achieve the steady combustion, but this study indicates that a slight variation of inflow parameters may induce the critical or unstable structures. Considering that the critical structure is still applicable in the engine, proposing a criterion on these two structures is necessary for the design. Furthermore, to contain these structures, the engine needs a relatively large combustor chamber. This jeopardizes the application potential of the ODW engine because several advantages root from its small size. Finally, the direct shift from the stable structure to the unstable structure, without the stage of the critical structure, suggests that stable operation of the ODW engine is very difficult in low Ma situations, deserving more attention in future work.

#### ACKNOWLEDGMENTS

This research was supported by the National Natural Science Foundation of China (NSFC) (Grant Nos. 11822202 and 91641130).

#### APPENDIX: GRID RESOLUTION VERIFICATION

The resolution study performed on the size scale is shown in Fig. 12 in which the temperature and pressure are obtained for  $M_0 = 7$  and  $L_t = 0$  and 5. [The corresponding temperature fields of these two cases are shown in Figs. 3(b) and 5(a).] To distinguish the effects of grid resolution, we quantitatively compare the temperature and pressure along different lines parallel with the  $x$ -axis. The black solid lines show the results for the grid number  $800 \times 300$ , and the dotted lines are the results computed with a half grid length by doubling the grid number to  $1000 \times 600$ . We see that the solid and dotted curves almost overlap with each other in Fig. 12, and the

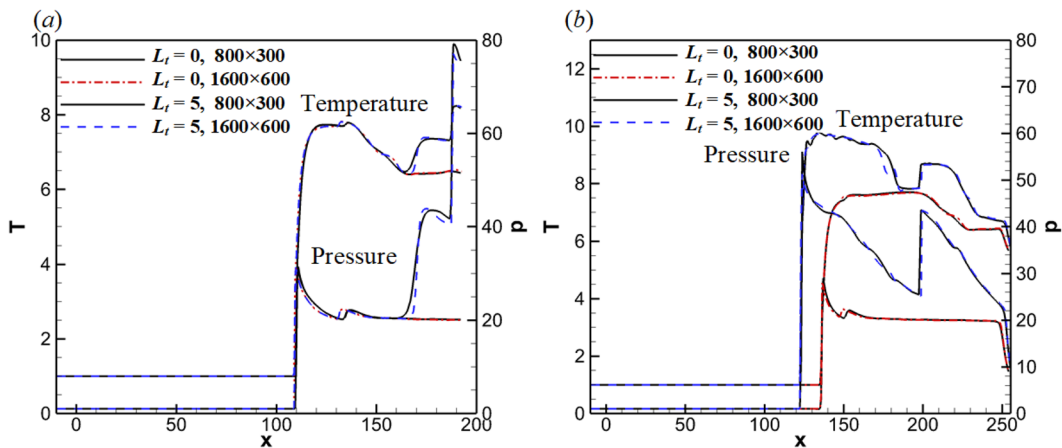


FIG. 12. Temperature and pressure along the line  $y = 90$  (a) and  $120$  (b) based on different grid scales for  $M_0 = 7$  and  $L_t = 0$  and  $5$ .

temperature and pressure do not change with the grid scale. The overall ODW dynamics is not affected.

The effect of grid size on the Mach stem surface was also investigated. Four grid numbers ( $400 \times 150$ ,  $800 \times 300$ ,  $1600 \times 600$ , and

$2400 \times 900$ ) were used for the case  $M_0 = 7$  and  $L_t = 5$ , and the results are shown in Fig. 13. A few transverse waves are generated along the Mach stem for all grid sizes, indicating a weakly unstable surface. Because the post-stem flow is subsonic, the disturbance

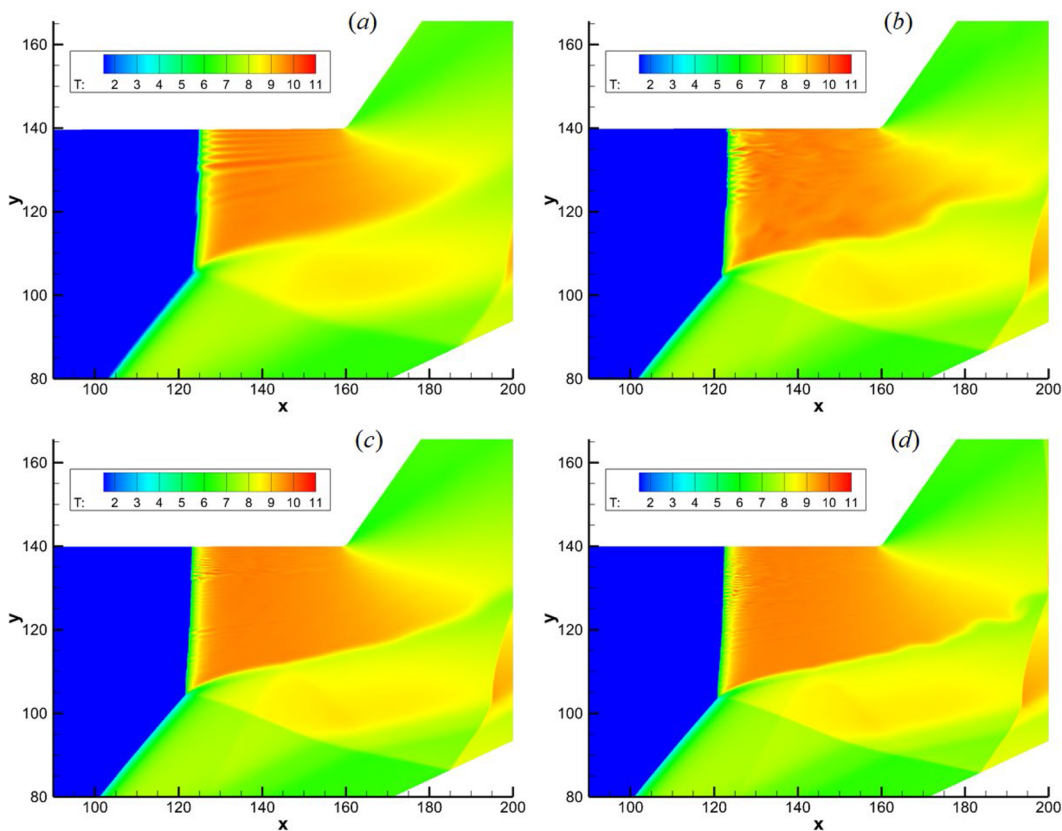


FIG. 13. Local temperature fields for  $M_0 = 7$  and  $L_t = 5$  for grid numbers  $400 \times 150$  (a),  $800 \times 300$  (b),  $1600 \times 600$  (c), and  $2400 \times 900$  (d).

from the lower and downstream boundary may travel upstream and destabilize the surface. The size of transverse waves decreases with improved grid accuracy, which means that the low grid resolution may not reflect the true transverse wave scale. However, the chosen grid size is sufficient to reveal the global structures for the purpose of this work.

## REFERENCES

- <sup>1</sup>E. T. Curran, W. H. Heiser, and D. T. Pratt, "Fluid phenomena in scramjet combustion systems," *Annu. Rev. Fluid Mech.* **28**, 323–360 (1996).
- <sup>2</sup>J. Urzay, "Supersonic combustion in air-breathing propulsion systems for hypersonic flight," *Annu. Rev. Fluid Mech.* **50**, 593–627 (2018).
- <sup>3</sup>Y. Tian, Y. Han, S. Yang, F. Zhong, and J. Le, "Investigation of fluctuating characteristics of wall shear stress in supersonic flow," *Phys. Fluids* **31**, 125110 (2019).
- <sup>4</sup>M. K. K. Devaraj, P. Jutur, S. M. V. Rao, G. Jagadeesh, and G. T. K. Anavardham, "Experimental investigation of unstart dynamics driven by subsonic spillage in a hypersonic scramjet intake at Mach 6," *Phys. Fluids* **32**, 026103 (2020).
- <sup>5</sup>C. Chen, T. Gao, and J. Liang, "Separation induced low-frequency unsteadiness in a supersonic combustor with single-side expansion," *Phys. Fluids* **31**, 056103 (2019).
- <sup>6</sup>G. D. Roy, S. M. Frolov, A. A. Borisov, and D. W. Netzer, "Pulse detonation propulsion: Challenges, current status, and future perspective," *Prog. Energy Combust. Sci.* **30**, 545–672 (2004).
- <sup>7</sup>P. Wolański, "Detonation propulsion," *Proc. Combust. Inst.* **34**, 125–158 (2013).
- <sup>8</sup>E. M. Braun, F. K. Lu, D. R. Wilson, and J. A. Camberos, "Airbreathing rotating detonation wave engine cycle analysis," *Aerosp. Sci. Technol.* **27**, 201–208 (2013).
- <sup>9</sup>Y. Liu, W. Zhou, Y. Yang, Z. Liu, and J. Wang, "Numerical study on the instabilities in H<sub>2</sub>-air rotating detonation engines," *Phys. Fluids* **30**, 046106 (2018).
- <sup>10</sup>H. F. Lehr, "Experiments on shock induced combustion," *Astronaut. Acta* **17**, 589–597 (1972).
- <sup>11</sup>A. Matsuo and T. Fujiwara, "Numerical investigation of oscillatory instability in shock-induced combustion around a blunt body," *AIAA J.* **31**, 1835–1841 (1993).
- <sup>12</sup>A. Matsuo and K. Fujii, "Detailed mechanism of the unsteady combustion around hypersonic projectiles," *AIAA J.* **34**, 2082–2089 (1996).
- <sup>13</sup>S. Maeda, J. Kasahara, and A. Matsuo, "Oblique detonation wave stability around a spherical projectile by a high time resolution optical observation," *Combust. Flame* **159**, 887–896 (2012).
- <sup>14</sup>S. Maeda, S. Sumiya, J. Kasahara, and A. Matsuo, "Initiation and sustaining mechanisms of stabilized Oblique Detonation Waves around projectiles," *Proc. Combust. Inst.* **34**, 1973–1980 (2013).
- <sup>15</sup>P. K. Pavalavanni, C. H. Sohn, B. J. Lee, and J.-Y. Choi, "Revisiting unsteady shock-induced combustion with modern analysis techniques," *Proc. Combust. Inst.* **37**, 3637–3644 (2019).
- <sup>16</sup>R. A. Gross, "Oblique detonation waves," *AIAA J.* **1**, 1225–1227 (1963).
- <sup>17</sup>D. T. Pratt, J. W. Humphrey, and D. E. Glenn, "Morphology of standing oblique detonation waves," *J. Propul. Power* **7**, 837–845 (1991).
- <sup>18</sup>C. Li, K. Kailasanath, and E. S. Oran, "Detonation structures behind oblique shocks," *Phys. Fluids* **6**, 1600–1611 (1994).
- <sup>19</sup>L. F. Figueira Da Silva and B. Deshaies, "Stabilization of an oblique detonation wave by a wedge: A parametric numerical study," *Combust. Flame* **121**, 152–166 (2000).
- <sup>20</sup>C. Viguier, L. F. Figueira Da Silva, D. Desbordes, and B. Deshaies, "Onset of oblique detonation waves: Comparison between experimental and numerical results for hydrogen-air mixtures," *Symp. (Int.) Combust.* **26**, 3023–3031 (1996).
- <sup>21</sup>H. H. Teng and Z. L. Jiang, "On the transition pattern of the oblique detonation structure," *J. Fluid Mech.* **713**, 659–669 (2012).
- <sup>22</sup>Y. Fang, Y. Zhang, X. Deng, and H. Teng, "Structure of wedge-induced oblique detonation in acetylene-oxygen-argon mixtures," *Phys. Fluids* **31**, 026108 (2019).
- <sup>23</sup>J.-Y. Choi, D.-W. Kim, I.-S. Jeung, F. Ma, and V. Yang, "Cell-like structure of unstable oblique detonation wave from high-resolution numerical simulation," *Proc. Combust. Inst.* **31**, 2473–2480 (2007).
- <sup>24</sup>J. Verreault, A. J. Higgins, and R. A. Stowe, "Formation of transverse waves in oblique detonations," *Proc. Combust. Inst.* **34**, 1913–1920 (2013).
- <sup>25</sup>H. H. Teng, Z. L. Jiang, and H. D. Ng, "Numerical study on unstable surfaces of oblique detonations," *J. Fluid Mech.* **744**, 111–128 (2014).
- <sup>26</sup>Y. Zhang, L. Zhou, J. Gong, H. D. Ng, and H. Teng, "Effects of activation energy on the instability of oblique detonation surfaces with a one-step chemistry model," *Phys. Fluids* **30**, 106110 (2018).
- <sup>27</sup>P. Yang, H. D. Ng, H. H. Teng, and Z. L. Jiang, "Initiation structure of oblique detonation waves behind conical shocks," *Phys. Fluids* **29**, 086104 (2017).
- <sup>28</sup>W. H. Han, C. Wang, and C. K. Law, "Three-dimensional simulation of oblique detonation waves attached to cone," *Phys. Rev. Fluids* **4**, 053201 (2019).
- <sup>29</sup>M. V. Papalexandris, "A numerical study of wedge-induced detonations," *Combust. Flame* **120**, 526 (2000).
- <sup>30</sup>J.-Y. Choi, E. J.-R. Shin, and I.-S. Jeung, "Unstable combustion induced by oblique shock waves at the non-attaching condition of the oblique detonation wave," *Proc. Combust. Inst.* **32**, 2387–2396 (2009).
- <sup>31</sup>Y. Liu, X. D. Han, S. B. Yao, and J. P. Wang, "A numerical investigation of the prompt oblique detonation wave sustained by a finite-length wedge," *Shock Waves* **26**, 729 (2016).
- <sup>32</sup>K. Ghorbanian and J. D. Sterling, "Influence of formation processes on oblique detonation wave stabilization," *J. Propul. Power* **12**, 509–517 (1996).
- <sup>33</sup>R. D. Dudebout, J. P. Sislian, and R. Oppitz, "Numerical simulation of hypersonic shock-induced combustion ramjets," *J. Propul. Power* **14**, 869–879 (1998).
- <sup>34</sup>J. P. Sislian, H. Schirmer, R. Dudebout, and J. Schumacher, "Propulsive performance of hypersonic oblique detonation wave and shock-induced combustion ramjets," *J. Propul. Power* **17**, 599–604 (2001).
- <sup>35</sup>H. D. Ng, M. I. Radulescu, A. J. Higgins, N. Nikiforakis, and J. H. S. Lee, "Numerical investigation of the instability for one-dimensional Chapman-Jouguet detonations with chain-branching kinetics," *Combust. Theory Model.* **9**, 385–401 (2005).
- <sup>36</sup>Y. Fang, Z. Zhang, and Z. Hu, "Effects of boundary layer on wedge-induced oblique detonation structures in hydrogen-air mixtures," *Int. J. Hydrogen Energy* **44**, 23429–23435 (2019).
- <sup>37</sup>H. Schlichting, *Boundary-Layer Theory*, 7th ed. (McGraw Hill, New York, USA, 1979), p. 638.
- <sup>38</sup>D. J. Acheson, *Elementary Fluid Dynamics*, Oxford Applied Mathematics and Computing Science Series, 2nd ed. (Clarendon Press, Oxford, UK, 1992).
- <sup>39</sup>K. H. Kim, C. Kim, and O.-H. Rho, "Methods for the accurate computations of hypersonic flows," *J. Comput. Phys.* **174**, 38–90 (2001).
- <sup>40</sup>P. Yang, H. H. Teng, Z. L. Jiang, and H. D. Ng, "Effects of inflow Mach number on oblique detonation initiation with a two-step induction-reaction kinetic model," *Combust. Flame* **193**, 246–256 (2018).
- <sup>41</sup>H. Li and G. Ben-Dor, "A parametric study of Mach reflection in steady flows," *J. Fluid Mech.* **341**, 101–125 (1997).
- <sup>42</sup>C. A. Mouton and H. G. Hornung, "Mach stem height and growth rate predictions," *AIAA J.* **45**, 1977–1987 (2007).